EUROPEAN ORGANIZATION FOR NUCLEAR RESEARCH (CERN)

CERN-PH-EP-2013-181
LHCb-PAPER-2013-049
January 6, 2014

Search for the doubly charmed baryon Ξ_{cc}^+

The LHCb collaboration[†]

Abstract

A search for the doubly charmed baryon Ξ_{cc}^+ in the decay mode $\Xi_{cc}^+ \to \Lambda_c^+ K^- \pi^+$ is performed with a data sample, corresponding to an integrated luminosity of 0.65 fb^{-1}, of pp collisions recorded at a centre-of-mass energy of 7 TeV. No significant signal is found in the mass range 3300–3800 MeV/c^2. Upper limits at the 95% confidence level on the ratio of the Ξ_{cc}^+ production cross-section times branching fraction to that of the Λ_c^+, R, are given as a function of the Ξ_{cc}^+ mass and lifetime. The largest upper limits range from $R < 1.5 \times 10^{-2}$ for a lifetime of 100 fs to $R < 3.9 \times 10^{-4}$ for a lifetime of 400 fs.

Published in JHEP, DOI: 10.1007/JHEP12(2013)090

[†]Authors are listed on the following pages.

LHCb collaboration

R. Aaij[40], B. Adeva[36], M. Adinolfi[45], C. Adrover[6], A. Affolder[51], Z. Ajaltouni[5], J. Albrecht[9], F. Alessio[37], M. Alexander[50], S. Ali[40], G. Alkhazov[29], P. Alvarez Cartelle[36], A.A. Alves Jr[24], S. Amato[2], S. Amerio[21], Y. Amhis[7], L. Anderlini[17,f], J. Anderson[39], R. Andreassen[56], J.E. Andrews[57], R.B. Appleby[53], O. Aquines Gutierrez[10], F. Archilli[18], A. Artamonov[34], M. Artuso[58], E. Aslanides[6], G. Auriemma[24,m], M. Baalouch[5], S. Bachmann[11], J.J. Back[47], A. Badalov[35], C. Baesso[59], V. Balagura[30], W. Baldini[16], R.J. Barlow[53], C. Barschel[37], S. Barsuk[7], W. Barter[46], Th. Bauer[40], A. Bay[38], J. Beddow[50], F. Bedeschi[22], I. Bediaga[1], S. Belogurov[30], K. Belous[34], I. Belyaev[30], E. Ben-Haim[8], G. Bencivenni[18], S. Benson[49], J. Benton[45], A. Berezhnoy[31], R. Bernet[39], M.-O. Bettler[46], M. van Beuzekom[40], A. Bien[11], S. Bifani[44], T. Bird[53], A. Bizzeti[17,h], P.M. Bjørnstad[53], T. Blake[37], F. Blanc[38], J. Blouw[10], S. Blusk[58], V. Bocci[24], A. Bondar[33], N. Bondar[29], W. Bonivento[15], S. Borghi[53], A. Borgia[58], T.J.V. Bowcock[51], E. Bowen[39], C. Bozzi[16], T. Brambach[9], J. van den Brand[41], J. Bressieux[38], D. Brett[53], M. Britsch[10], T. Britton[58], N.H. Brook[45], H. Brown[51], A. Bursche[39], G. Busetto[21,q], J. Buytaert[37], S. Cadeddu[15], O. Callot[7], M. Calvi[20,j], M. Calvo Gomez[35,n], A. Camboni[35], P. Campana[18,37], D. Campora Perez[37], A. Carbone[14,c], G. Carboni[23,k], R. Cardinale[19,i], A. Cardini[15], H. Carranza-Mejia[49], L. Carson[52], K. Carvalho Akiba[2], G. Casse[51], L. Castillo Garcia[37], M. Cattaneo[37], Ch. Cauet[9], R. Cenci[57], M. Charles[8], Ph. Charpentier[37], S.-F. Cheung[54], N. Chiapolini[39], M. Chrzaszcz[39,25], K. Ciba[37], X. Cid Vidal[37], G. Ciezarek[52], P.E.L. Clarke[49], M. Clemencic[37], H.V. Cliff[46], J. Closier[37], C. Coca[28], V. Coco[40], J. Cogan[6], E. Cogneras[5], P. Collins[37], A. Comerma-Montells[35], A. Contu[15,37], A. Cook[45], M. Coombes[45], S. Coquereau[8], G. Corti[37], B. Couturier[37], G.A. Cowan[49], D.C. Craik[47], M. Cruz Torres[59], S. Cunliffe[52], R. Currie[49], C. D'Ambrosio[37], P. David[8], P.N.Y. David[40], A. Davis[56], I. De Bonis[4], K. De Bruyn[40], S. De Capua[53], M. De Cian[11], J.M. De Miranda[1], L. De Paula[2], W. De Silva[56], P. De Simone[18], D. Decamp[4], M. Deckenhoff[9], L. Del Buono[8], N. Déléage[4], D. Derkach[54], O. Deschamps[5], F. Dettori[41], A. Di Canto[11], H. Dijkstra[37], M. Dogaru[28], S. Donleavy[51], F. Dordei[11], A. Dosil Suárez[36], D. Dossett[47], A. Dovbnya[42], F. Dupertuis[38], P. Durante[37], R. Dzhelyadin[34], A. Dziurda[25], A. Dzyuba[29], S. Easo[48], U. Egede[52], V. Egorychev[30], S. Eidelman[33], D. van Eijk[40], S. Eisenhardt[49], U. Eitschberger[9], R. Ekelhof[9], L. Eklund[50,37], I. El Rifai[5], Ch. Elsasser[39], A. Falabella[14,e], C. Färber[11], C. Farinelli[40], S. Farry[51], D. Ferguson[49], V. Fernandez Albor[36], F. Ferreira Rodrigues[1], M. Ferro-Luzzi[37], S. Filippov[32], M. Fiore[16,e], C. Fitzpatrick[37], M. Fontana[10], F. Fontanelli[19,i], R. Forty[37], O. Francisco[2], M. Frank[37], C. Frei[37], M. Frosini[17,37,f], E. Furfaro[23,k], A. Gallas Torreira[36], D. Galli[14,c], M. Gandelman[2], P. Gandini[58], Y. Gao[3], J. Garofoli[58], P. Garosi[53], J. Garra Tico[46], L. Garrido[35], C. Gaspar[37], R. Gauld[54], E. Gersabeck[11], M. Gersabeck[53], T. Gershon[47], Ph. Ghez[4], V. Gibson[46], L. Giubega[28], V.V. Gligorov[37], C. Göbel[59], D. Golubkov[30], A. Golutvin[52,30,37], A. Gomes[2], P. Gorbounov[30,37], H. Gordon[37], M. Grabalosa Gándara[5], R. Graciani Diaz[35], L.A. Granado Cardoso[37], E. Graugés[35], G. Graziani[17], A. Grecu[28], E. Greening[54], S. Gregson[46], P. Griffith[44], L. Grillo[11], O. Grünberg[60], B. Gui[58], E. Gushchin[32], Yu. Guz[34,37], T. Gys[37], C. Hadjivasiliou[58], G. Haefeli[38], C. Haen[37], S.C. Haines[46], S. Hall[52], B. Hamilton[57], T. Hampson[45], S. Hansmann-Menzemer[11], N. Harnew[54], S.T. Harnew[45], J. Harrison[53], T. Hartmann[60], J. He[37], T. Head[37], V. Heijne[40], K. Hennessy[51], P. Henrard[5], J.A. Hernando Morata[36], E. van Herwijnen[37], M. Heß[60], A. Hicheur[1], E. Hicks[51], D. Hill[54], M. Hoballah[5], C. Hombach[53], W. Hulsbergen[40], P. Hunt[54], T. Huse[51], N. Hussain[54], D. Hutchcroft[51], D. Hynds[50], V. Iakovenko[43], M. Idzik[26], P. Ilten[12], R. Jacobsson[37], A. Jaeger[11],

E. Jans[40], P. Jaton[38], A. Jawahery[57], F. Jing[3], M. John[54], D. Johnson[54], C.R. Jones[46], C. Joram[37], B. Jost[37], M. Kaballo[9], S. Kandybei[42], W. Kanso[6], M. Karacson[37], T.M. Karbach[37], I.R. Kenyon[44], T. Ketel[41], B. Khanji[20], O. Kochebina[7], I. Komarov[38], R.F. Koopman[41], P. Koppenburg[40], M. Korolev[31], A. Kozlinskiy[40], L. Kravchuk[32], K. Kreplin[11], M. Kreps[47], G. Krocker[11], P. Krokovny[33], F. Kruse[9], M. Kucharczyk[20,25,37,j], V. Kudryavtsev[33], K. Kurek[27], T. Kvaratskheliya[30,37], V.N. La Thi[38], D. Lacarrere[37], G. Lafferty[53], A. Lai[15], D. Lambert[49], R.W. Lambert[41], E. Lanciotti[37], G. Lanfranchi[18], C. Langenbruch[37], T. Latham[47], C. Lazzeroni[44], R. Le Gac[6], J. van Leerdam[40], J.-P. Lees[4], R. Lefèvre[5], A. Leflat[31], J. Lefrançois[7], S. Leo[22], O. Leroy[6], T. Lesiak[25], B. Leverington[11], Y. Li[3], L. Li Gioi[5], M. Liles[51], R. Lindner[37], C. Linn[11], B. Liu[3], G. Liu[37], S. Lohn[37], I. Longstaff[50], J.H. Lopes[2], N. Lopez-March[38], H. Lu[3], D. Lucchesi[21,q], J. Luisier[38], H. Luo[49], O. Lupton[54], F. Machefert[7], I.V. Machikhiliyan[30], F. Maciuc[28], O. Maev[29,37], S. Malde[54], G. Manca[15,d], G. Mancinelli[6], J. Maratas[5], U. Marconi[14], P. Marino[22,s], R. Märki[38], J. Marks[11], G. Martellotti[24], A. Martens[8], A. Martín Sánchez[7], M. Martinelli[40], D. Martinez Santos[41,37], D. Martins Tostes[2], A. Martynov[31], A. Massafferri[1], R. Matev[37], Z. Mathe[37], C. Matteuzzi[20], E. Maurice[6], A. Mazurov[16,37,e], J. McCarthy[44], A. McNab[53], R. McNulty[12], B. McSkelly[51], B. Meadows[56,54], F. Meier[9], M. Meissner[11], M. Merk[40], D.A. Milanes[8], M.-N. Minard[4], J. Molina Rodriguez[59], S. Monteil[5], D. Moran[53], P. Morawski[25], A. Mordà[6], M.J. Morello[22,s], R. Mountain[58], I. Mous[40], F. Muheim[49], K. Müller[39], R. Muresan[28], B. Muryn[26], B. Muster[38], P. Naik[45], T. Nakada[38], R. Nandakumar[48], I. Nasteva[1], M. Needham[49], S. Neubert[37], N. Neufeld[37], A.D. Nguyen[38], T.D. Nguyen[38], C. Nguyen-Mau[38,o], M. Nicol[7], V. Niess[5], R. Niet[9], N. Nikitin[31], T. Nikodem[11], A. Nomerotski[54], A. Novoselov[34], A. Oblakowska-Mucha[26], V. Obraztsov[34], S. Oggero[40], S. Ogilvy[50], O. Okhrimenko[43], R. Oldeman[15,d], M. Orlandea[28], J.M. Otalora Goicochea[2], P. Owen[52], A. Oyanguren[35], B.K. Pal[58], A. Palano[13,b], M. Palutan[18], J. Panman[37], A. Papanestis[48], M. Pappagallo[50], C. Parkes[53], C.J. Parkinson[52], G. Passaleva[17], G.D. Patel[51], M. Patel[52], G.N. Patrick[48], C. Patrignani[19,i], C. Pavel-Nicorescu[28], A. Pazos Alvarez[36], A. Pearce[53], A. Pellegrino[40], G. Penso[24,l], M. Pepe Altarelli[37], S. Perazzini[14,c], E. Perez Trigo[36], A. Pérez-Calero Yzquierdo[35], P. Perret[5], M. Perrin-Terrin[6], L. Pescatore[44], E. Pesen[61], G. Pessina[20], K. Petridis[52], A. Petrolini[19,i], A. Phan[58], E. Picatoste Olloqui[35], B. Pietrzyk[4], T. Pilař[47], D. Pinci[24], S. Playfer[49], M. Plo Casasus[36], F. Polci[8], G. Polok[25], A. Poluektov[47,33], E. Polycarpo[2], A. Popov[34], D. Popov[10], B. Popovici[28], C. Potterat[35], A. Powell[54], J. Prisciandaro[38], A. Pritchard[51], C. Prouve[7], V. Pugatch[43], A. Puig Navarro[38], G. Punzi[22,r], W. Qian[4], B. Rachwal[25], J.H. Rademacker[45], B. Rakotomiaramanana[38], M.S. Rangel[2], I. Raniuk[42], N. Rauschmayr[37], G. Raven[41], S. Redford[54], S. Reichert[53], M.M. Reid[47], A.C. dos Reis[1], S. Ricciardi[48], A. Richards[52], K. Rinnert[51], V. Rives Molina[35], D.A. Roa Romero[5], P. Robbe[7], D.A. Roberts[57], A.B. Rodrigues[1], E. Rodrigues[53], P. Rodriguez Perez[36], S. Roiser[37], V. Romanovsky[34], A. Romero Vidal[36], M. Rotondo[21], J. Rouvinet[38], T. Ruf[37], F. Ruffini[22], H. Ruiz[35], P. Ruiz Valls[35], G. Sabatino[24,k], J.J. Saborido Silva[36], N. Sagidova[29], P. Sail[50], B. Saitta[15,d], V. Salustino Guimaraes[2], B. Sanmartin Sedes[36], R. Santacesaria[24], C. Santamarina Rios[36], E. Santovetti[23,k], M. Sapunov[6], A. Sarti[18], C. Satriano[24,m], A. Satta[23], M. Savrie[16,e], D. Savrina[30,31], M. Schiller[41], H. Schindler[37], M. Schlupp[9], M. Schmelling[10], B. Schmidt[37], O. Schneider[38], A. Schopper[37], M.-H. Schune[7], R. Schwemmer[37], B. Sciascia[18], A. Sciubba[24], M. Seco[36], A. Semennikov[30], K. Senderowska[26], I. Sepp[52], N. Serra[39], J. Serrano[6], P. Seyfert[11], M. Shapkin[34], I. Shapoval[16,42,e], Y. Shcheglov[29], T. Shears[51], L. Shekhtman[33], O. Shevchenko[42], V. Shevchenko[30], A. Shires[9], R. Silva Coutinho[47], M. Sirendi[46], N. Skidmore[45], T. Skwarnicki[58],

N.A. Smith[51], E. Smith[54,48], E. Smith[52], J. Smith[46], M. Smith[53], M.D. Sokoloff[56], F.J.P. Soler[50], F. Soomro[38], D. Souza[45], B. Souza De Paula[2], B. Spaan[9], A. Sparkes[49], P. Spradlin[50], F. Stagni[37], S. Stahl[11], O. Steinkamp[39], S. Stevenson[54], S. Stoica[28], S. Stone[58], B. Storaci[39], M. Straticiuc[28], U. Straumann[39], V.K. Subbiah[37], L. Sun[56], W. Sutcliffe[52], S. Swientek[9], V. Syropoulos[41], M. Szczekowski[27], P. Szczypka[38,37], D. Szilard[2], T. Szumlak[26], S. T'Jampens[4], M. Teklishyn[7], E. Teodorescu[28], F. Teubert[37], C. Thomas[54], E. Thomas[37], J. van Tilburg[11], V. Tisserand[4], M. Tobin[38], S. Tolk[41], D. Tonelli[37], S. Topp-Joergensen[54], N. Torr[54], E. Tournefier[4,52], S. Tourneur[38], M.T. Tran[38], M. Tresch[39], A. Tsaregorodtsev[6], P. Tsopelas[40], N. Tuning[40,37], M. Ubeda Garcia[37], A. Ukleja[27], A. Ustyuzhanin[52,p], U. Uwer[11], V. Vagnoni[14], G. Valenti[14], A. Vallier[7], R. Vazquez Gomez[18], P. Vazquez Regueiro[36], C. Vázquez Sierra[36], S. Vecchi[16], J.J. Velthuis[45], M. Veltri[17,g], G. Veneziano[38], M. Vesterinen[37], B. Viaud[7], D. Vieira[2], X. Vilasis-Cardona[35,n], A. Vollhardt[39], D. Volyanskyy[10], D. Voong[45], A. Vorobyev[29], V. Vorobyev[33], C. Voß[60], H. Voss[10], R. Waldi[60], C. Wallace[47], R. Wallace[12], S. Wandernoth[11], J. Wang[58], D.R. Ward[46], N.K. Watson[44], A.D. Webber[53], D. Websdale[52], M. Whitehead[47], J. Wicht[37], J. Wiechczynski[25], D. Wiedner[11], L. Wiggers[40], G. Wilkinson[54], M.P. Williams[47,48], M. Williams[55], F.F. Wilson[48], J. Wimberley[57], J. Wishahi[9], W. Wislicki[27], M. Witek[25], G. Wormser[7], S.A. Wotton[46], S. Wright[46], S. Wu[3], K. Wyllie[37], Y. Xie[49,37], Z. Xing[58], Z. Yang[3], X. Yuan[3], O. Yushchenko[34], M. Zangoli[14], M. Zavertyaev[10,a], F. Zhang[3], L. Zhang[58], W.C. Zhang[12], Y. Zhang[3], A. Zhelezov[11], A. Zhokhov[30], L. Zhong[3], A. Zvyagin[37].

[1] *Centro Brasileiro de Pesquisas Físicas (CBPF), Rio de Janeiro, Brazil*
[2] *Universidade Federal do Rio de Janeiro (UFRJ), Rio de Janeiro, Brazil*
[3] *Center for High Energy Physics, Tsinghua University, Beijing, China*
[4] *LAPP, Université de Savoie, CNRS/IN2P3, Annecy-Le-Vieux, France*
[5] *Clermont Université, Université Blaise Pascal, CNRS/IN2P3, LPC, Clermont-Ferrand, France*
[6] *CPPM, Aix-Marseille Université, CNRS/IN2P3, Marseille, France*
[7] *LAL, Université Paris-Sud, CNRS/IN2P3, Orsay, France*
[8] *LPNHE, Université Pierre et Marie Curie, Université Paris Diderot, CNRS/IN2P3, Paris, France*
[9] *Fakultät Physik, Technische Universität Dortmund, Dortmund, Germany*
[10] *Max-Planck-Institut für Kernphysik (MPIK), Heidelberg, Germany*
[11] *Physikalisches Institut, Ruprecht-Karls-Universität Heidelberg, Heidelberg, Germany*
[12] *School of Physics, University College Dublin, Dublin, Ireland*
[13] *Sezione INFN di Bari, Bari, Italy*
[14] *Sezione INFN di Bologna, Bologna, Italy*
[15] *Sezione INFN di Cagliari, Cagliari, Italy*
[16] *Sezione INFN di Ferrara, Ferrara, Italy*
[17] *Sezione INFN di Firenze, Firenze, Italy*
[18] *Laboratori Nazionali dell'INFN di Frascati, Frascati, Italy*
[19] *Sezione INFN di Genova, Genova, Italy*
[20] *Sezione INFN di Milano Bicocca, Milano, Italy*
[21] *Sezione INFN di Padova, Padova, Italy*
[22] *Sezione INFN di Pisa, Pisa, Italy*
[23] *Sezione INFN di Roma Tor Vergata, Roma, Italy*
[24] *Sezione INFN di Roma La Sapienza, Roma, Italy*
[25] *Henryk Niewodniczanski Institute of Nuclear Physics Polish Academy of Sciences, Kraków, Poland*
[26] *AGH - University of Science and Technology, Faculty of Physics and Applied Computer Science, Kraków, Poland*
[27] *National Center for Nuclear Research (NCBJ), Warsaw, Poland*
[28] *Horia Hulubei National Institute of Physics and Nuclear Engineering, Bucharest-Magurele, Romania*
[29] *Petersburg Nuclear Physics Institute (PNPI), Gatchina, Russia*

[30] *Institute of Theoretical and Experimental Physics (ITEP), Moscow, Russia*
[31] *Institute of Nuclear Physics, Moscow State University (SINP MSU), Moscow, Russia*
[32] *Institute for Nuclear Research of the Russian Academy of Sciences (INR RAN), Moscow, Russia*
[33] *Budker Institute of Nuclear Physics (SB RAS) and Novosibirsk State University, Novosibirsk, Russia*
[34] *Institute for High Energy Physics (IHEP), Protvino, Russia*
[35] *Universitat de Barcelona, Barcelona, Spain*
[36] *Universidad de Santiago de Compostela, Santiago de Compostela, Spain*
[37] *European Organization for Nuclear Research (CERN), Geneva, Switzerland*
[38] *Ecole Polytechnique Fédérale de Lausanne (EPFL), Lausanne, Switzerland*
[39] *Physik-Institut, Universität Zürich, Zürich, Switzerland*
[40] *Nikhef National Institute for Subatomic Physics, Amsterdam, The Netherlands*
[41] *Nikhef National Institute for Subatomic Physics and VU University Amsterdam, Amsterdam, The Netherlands*
[42] *NSC Kharkiv Institute of Physics and Technology (NSC KIPT), Kharkiv, Ukraine*
[43] *Institute for Nuclear Research of the National Academy of Sciences (KINR), Kyiv, Ukraine*
[44] *University of Birmingham, Birmingham, United Kingdom*
[45] *H.H. Wills Physics Laboratory, University of Bristol, Bristol, United Kingdom*
[46] *Cavendish Laboratory, University of Cambridge, Cambridge, United Kingdom*
[47] *Department of Physics, University of Warwick, Coventry, United Kingdom*
[48] *STFC Rutherford Appleton Laboratory, Didcot, United Kingdom*
[49] *School of Physics and Astronomy, University of Edinburgh, Edinburgh, United Kingdom*
[50] *School of Physics and Astronomy, University of Glasgow, Glasgow, United Kingdom*
[51] *Oliver Lodge Laboratory, University of Liverpool, Liverpool, United Kingdom*
[52] *Imperial College London, London, United Kingdom*
[53] *School of Physics and Astronomy, University of Manchester, Manchester, United Kingdom*
[54] *Department of Physics, University of Oxford, Oxford, United Kingdom*
[55] *Massachusetts Institute of Technology, Cambridge, MA, United States*
[56] *University of Cincinnati, Cincinnati, OH, United States*
[57] *University of Maryland, College Park, MD, United States*
[58] *Syracuse University, Syracuse, NY, United States*
[59] *Pontifícia Universidade Católica do Rio de Janeiro (PUC-Rio), Rio de Janeiro, Brazil, associated to* [2]
[60] *Institut für Physik, Universität Rostock, Rostock, Germany, associated to* [11]
[61] *Celal Bayar University, Manisa, Turkey, associated to* [37]

[a] *P.N. Lebedev Physical Institute, Russian Academy of Science (LPI RAS), Moscow, Russia*
[b] *Università di Bari, Bari, Italy*
[c] *Università di Bologna, Bologna, Italy*
[d] *Università di Cagliari, Cagliari, Italy*
[e] *Università di Ferrara, Ferrara, Italy*
[f] *Università di Firenze, Firenze, Italy*
[g] *Università di Urbino, Urbino, Italy*
[h] *Università di Modena e Reggio Emilia, Modena, Italy*
[i] *Università di Genova, Genova, Italy*
[j] *Università di Milano Bicocca, Milano, Italy*
[k] *Università di Roma Tor Vergata, Roma, Italy*
[l] *Università di Roma La Sapienza, Roma, Italy*
[m] *Università della Basilicata, Potenza, Italy*
[n] *LIFAELS, La Salle, Universitat Ramon Llull, Barcelona, Spain*
[o] *Hanoi University of Science, Hanoi, Viet Nam*
[p] *Institute of Physics and Technology, Moscow, Russia*
[q] *Università di Padova, Padova, Italy*
[r] *Università di Pisa, Pisa, Italy*

[s] *Scuola Normale Superiore, Pisa, Italy*

1 Introduction

The constituent quark model [1–3] predicts the existence of multiplets of baryon and meson states, with a structure determined by the symmetry properties of the hadron wavefunctions. When considering u, d, s, and c quarks, the states form $SU(4)$ multiplets [4]. The baryon ground states—those with no orbital or radial excitations—consist of a 20-plet with spin-parity $J^P = 1/2^+$ and a 20-plet with $J^P = 3/2^+$. All of the ground states with charm quantum number $C = 0$ or $C = 1$ have been discovered [5]. Three weakly decaying $C = 2$ states are expected: a Ξ_{cc} isodoublet (ccu, ccd) and an Ω_{cc} isosinglet (ccs), each with $J^P = 1/2^+$. This paper reports a search for the Ξ_{cc}^+ baryon. There are numerous predictions for the masses of these states (see, *e.g.*, Ref. [6] and the references therein, as well as Refs. [7–11]) with most estimates for the Ξ_{cc}^+ mass in the range 3500–3700 MeV/c^2. Predictions for its lifetime range between 100 and 250 fs [12–14].

Signals for the Ξ_{cc}^+ baryon were reported in the $\Lambda_c^+ K^- \pi^+$ and pD^+K^- final states by the SELEX collaboration, using a hyperon beam (containing an admixture of p, Σ^-, and π^-) on a fixed target [15, 16]. The mass was measured to be 3519 ± 2 MeV/c^2, and the lifetime was found to be compatible with zero within experimental resolution and less than 33 fs at the 90% confidence level (CL). SELEX estimated that 20% of their Λ_c^+ yield originates from Ξ_{cc}^+ decays, in contrast to theory expectations that the production of doubly charmed baryons would be suppressed by several orders of magnitude with respect to singly charmed baryons [17]. Searches in different production environments at the FOCUS, BaBar, and Belle experiments have not shown evidence for a Ξ_{cc}^+ state with the properties reported by SELEX [18–20].

This paper presents the result of a search for the decay[1] $\Xi_{cc}^+ \to \Lambda_c^+ K^- \pi^+$ with the LHCb detector and an integrated luminosity of 0.65 fb^{-1} of pp collision data recorded at centre-of-mass energy $\sqrt{s} = 7$ TeV. Double charm production has been observed previously at LHCb both in the $J/\psi\, J/\psi$ final state [21] and in final states including one or two open charm hadrons [22]. Phenomenological estimates of the production cross-section of Ξ_{cc} in pp collisions at $\sqrt{s} = 14$ TeV are in the range 60–1800 nb [17, 23, 24]; the cross-section at $\sqrt{s} = 7$ TeV is expected to be roughly a factor of two smaller. As is typical for charmed hadrons, the production is expected to be concentrated in the low transverse momentum ($p_{\rm T}$) and forward rapidity (y) kinematic region instrumented by LHCb [24]. For comparison, the prompt Λ_c^+ cross-section in the range $0 < p_{\rm T} < 8000$ MeV/c and $2.0 < y < 4.5$ at $\sqrt{s} = 7$ TeV has been measured to be $(233 \pm 26 \pm 71 \pm 14)$ μb at LHCb [25], where the uncertainties are statistical, systematic, and due to the description of the fragmentation model, respectively. Thus, the cross-section for Ξ_{cc}^+ production at LHCb is predicted to be smaller than that for Λ_c^+ by a factor of order 10^{-4} to 10^{-3}.

To reduce systematic uncertainties, the Ξ_{cc}^+ cross-section is measured relative to that of the Λ_c^+. This has the further advantage that it allows a direct comparison with previous

[1] The inclusion of charge-conjugate processes is implied throughout.

experimental results. The production ratio R that is measured is defined as

$$R \equiv \frac{\sigma(\Xi_{cc}^+)\,\mathcal{B}(\Xi_{cc}^+ \to \Lambda_c^+ K^-\pi^+)}{\sigma(\Lambda_c^+)} = \frac{N_{\rm sig}}{N_{\rm norm}}\frac{\varepsilon_{\rm norm}}{\varepsilon_{\rm sig}}, \tag{1}$$

where $N_{\rm sig}$ and $N_{\rm norm}$ refer to the measured yields of the signal (Ξ_{cc}^+) and normalisation (Λ_c^+) modes, $\varepsilon_{\rm sig}$ and $\varepsilon_{\rm norm}$ are the corresponding efficiencies, $\mathcal{B}$ indicates a branching fraction, and σ indicates a cross-section. Assuming that $\mathcal{B}(\Xi_{cc}^+ \to \Lambda_c^+ K^-\pi^+) \approx \mathcal{B}(\Lambda_c^+ \to pK^-\pi^+) \approx 5\%$ [5], the expected value of R at LHCb is of order 10^{-5} to 10^{-4}. By contrast, the SELEX observation [15] reported 15.9 Ξ_{cc}^+ signal events in a sample of 1630 Λ_c^+ events with an efficiency ratio of 11%, corresponding to $R = 9\%$. For convenience, the single-event sensitivity α is defined as

$$\alpha \equiv \frac{\varepsilon_{\rm norm}}{N_{\rm norm}\,\varepsilon_{\rm sig}} \tag{2}$$

such that $R = \alpha N_{\rm sig}$. For each candidate the mass difference δm is computed as

$$\delta m \equiv m([pK^-\pi^+]_{\Lambda_c}K^-\pi^+) - m([pK^-\pi^+]_{\Lambda_c}) - m(K^-) - m(\pi^+), \tag{3}$$

where $m([pK^-\pi^+]_{\Lambda_c}K^-\pi^+)$ is the measured invariant mass of the Ξ_{cc}^+ candidate, $m([pK^-\pi^+]_{\Lambda_c})$ is the measured invariant mass of the $pK^-\pi^+$ combination forming the Λ_c^+ candidate, and $m(K^-)$ and $m(\pi^+)$ are the world-average masses of charged kaons and pions, respectively [5].

Since no assumption is made about the Ξ_{cc}^+ mass, a wide signal window of $380 < \delta m < 880\,{\rm MeV}/c^2$ is used for this search, corresponding to approximately $3300 < m(\Xi_{cc}^+) < 3800\,{\rm MeV}/c^2$. All aspects of the analysis procedure were fixed before the data in this signal region were examined. Limits on R are quoted as a function of the Ξ_{cc}^+ mass and lifetime, since the measured yield depends on δm, and $\varepsilon_{\rm sig}$ depends on both the mass and lifetime.

2 Detector and software

The LHCb detector [26] is a single-arm forward spectrometer covering the pseudorapidity range $2 < \eta < 5$, designed for the study of particles containing b or c quarks. The detector includes a high-precision tracking system consisting of a silicon-strip vertex detector (VELO) surrounding the pp interaction region, a large-area silicon-strip detector located upstream of a dipole magnet with a bending power of about 4 Tm, and three stations of silicon-strip detectors and straw drift tubes placed downstream. The combined tracking system provides a momentum measurement with relative uncertainty that varies from 0.4% at 5 GeV/c to 0.6% at 100 GeV/c, and impact parameter (IP) resolution of 20 μm for tracks with large transverse momentum. Charged hadrons are identified using two ring-imaging Cherenkov detectors [27]. Photon, electron, and hadron candidates are identified by a calorimeter system consisting of scintillating-pad and preshower detectors, an electromagnetic calorimeter, and a hadronic calorimeter. Muons are identified by a system composed of alternating layers of iron and multiwire proportional chambers [28].

The trigger [29] consists of a hardware stage, based on information from the calorimeter and muon systems, followed by a software stage, which applies a full event reconstruction.

In the simulation, pp collisions are generated using Pythia 6.4 [30] with a specific LHCb configuration [31]. A dedicated generator, Genxicc v2.0, is used to simulate Ξ_{cc}^+ baryon production [32]. Decays of hadronic particles are described by EvtGen [33], in which final state radiation is generated using Photos [34]. The interaction of the generated particles with the detector and its response are implemented using the Geant4 toolkit [35] as described in Ref. [36]. Unless otherwise stated, simulated events are generated with $m(\Xi_{cc}^+) = 3500\,\mathrm{MeV}/c^2$, with $\tau_{\Xi_{cc}^+} = 333\,\mathrm{fs}$, and with the Ξ_{cc}^+ and Λ_c^+ decay products distributed according to phase space.

3 Triggering, reconstruction, and selection

The procedure to trigger, reconstruct, and select candidates for the signal and normalisation modes is designed to retain signal and to suppress three primary sources of background. These are combinations of unrelated tracks, especially those originating from the same primary interaction vertex (PV); mis-reconstructed charm or beauty hadron decays, which typically occur at a displaced vertex; and combinations of a real Λ_c^+ with other tracks to form a fake Ξ_{cc}^+ candidate. The first two classes generally have a smooth distribution in both $m([pK^-\pi^+]_{\Lambda_c})$ and δm; the third peaks in $m([pK^-\pi^+]_{\Lambda_c})$ but is smooth in δm.

For both the Ξ_{cc}^+ search and the normalisation mode, Λ_c^+ candidates are reconstructed in the final state $pK^-\pi^+$. To minimise systematic differences in efficiency between the signal and normalisation modes, the same trigger requirements are used for both modes, and those requirements ensure that the event was triggered by the Λ_c^+ candidate and its daughter tracks. First, at least one of the three Λ_c^+ daughter tracks must correspond to a calorimeter cluster with a measured transverse energy $E_{\mathrm{T}} > 3500\,\mathrm{MeV}$ in the hardware trigger. Second, at least one of the three Λ_c^+ daughter tracks must be selected by the inclusive software trigger, which requires that the track have $p_{\mathrm{T}} > 1700\,\mathrm{MeV}/c$ and $\chi^2_{\mathrm{IP}} > 16$ with respect to any PV, where χ^2_{IP} is defined as the difference in χ^2 of a given PV reconstructed with and without the considered track. Third, the Λ_c^+ candidate must be reconstructed and accepted by a dedicated $\Lambda_c^+ \to pK^-\pi^+$ selection algorithm in the software trigger. This algorithm makes several geometric and kinematic requirements, the most important of which are as follows. The three daughter tracks are required to have $p_{\mathrm{T}} > 500\,\mathrm{MeV}/c^2$, to have a track fit $\chi^2/\mathrm{ndf} < 3$, not to originate at a PV ($\chi^2_{\mathrm{IP}} > 16$), and to meet at a common vertex ($\chi^2/\mathrm{ndf} < 15$, where ndf is the number of degrees of freedom). The Λ_c^+ candidate formed from the three tracks is required to have $p_{\mathrm{T}} > 2500\,\mathrm{MeV}/c^2$, to lie within the mass window $2150 < m([pK^-\pi^+]_{\Lambda_c}) < 2430\,\mathrm{MeV}/c^2$, to be significantly displaced from the PV (vertex separation $\chi^2 > 16$), and to point back towards the PV (momentum and displacement vectors within 1°). The software trigger also requires that the proton candidate be inconsistent with the pion and kaon mass hypotheses. The Λ_c^+ trigger algorithm was only enabled for part of the data-taking in 2011, corresponding to an integrated luminosity of $0.65\,\mathrm{fb}^{-1}$.

For events that pass the trigger, the Λ_c^+ selection proceeds in a similar fashion to that used in the software trigger: three charged tracks are required to form a common vertex that is significantly displaced from the event PV and has invariant mass in the range $2185 < m([pK^-\pi^+]_{\Lambda_c}) < 2385\,\mathrm{MeV}/c^2$. Particle identification (PID) requirements are imposed on all three tracks to suppress combinatorial background and mis-identified charm meson decays. The same Λ_c^+ selection is used for the signal and normalisation modes.

The Ξ_{cc}^+ candidates are formed by combining a Λ_c^+ candidate with two tracks, one identified as a K^- and one as a π^+. These three particles are required to form a common vertex ($\chi^2/\mathrm{ndf} < 10$) that is displaced from the PV (vertex separation $\chi^2 > 16$). The kaon and pion daughter tracks are also required to not originate at the PV ($\chi^2_{\mathrm{IP}} > 16$) and to have $p_{\mathrm{T}} > 250\,\mathrm{MeV}/c$. The Ξ_{cc}^+ candidate is required to point back to the PV and to have $p_{\mathrm{T}} > 2000\,\mathrm{MeV}/c$.

A multivariate selection is applied only to the signal mode to further improve the purity. The selector used is an artificial neural network (ANN) implemented in the TMVA package [37]. The input variables are chosen to have limited dependence on the Ξ_{cc}^+ lifetime. To train the selector, simulated Ξ_{cc}^+ decays are used as the signal sample and 3.5% of the candidates from δm sidebands of width $200\,\mathrm{MeV}/c^2$ adjacent to the signal region are used as the background sample. In order to increase the available statistics, the trigger requirements are relaxed for these samples. In addition to the training samples, disjoint test samples of equal size are taken from the same sources. After training, the response distribution of the ANN is compared between the training and test samples. Good agreement is found for both signal and background, with Kolmogorov-Smirnov test p-values of 80% and 65%, respectively. A selection cut on the ANN response is applied to the data used in the Ξ_{cc}^+ search. In the test samples, the efficiency of this requirement is 55.7% for signal and 4.2% for background.

The selection has limited efficiency for short-lived Ξ_{cc}^+. This is principally due to the requirements that the Ξ_{cc}^+ decay vertex be significantly displaced from the PV, and that the Ξ_{cc}^+ daughter kaon and pion have a significant impact parameter with respect to the PV. As a consequence, the analysis is insensitive to Ξ_c resonances that decay strongly to the same final state, notably the $\Xi_c(2980)^+$, $\Xi_c(3055)^+$, and $\Xi_c(3080)^+$ [20, 38].

4 Yield measurements

To determine the Λ_c^+ yield, N_{norm}, a fit is performed to the $pK^-\pi^+$ mass spectrum. The signal shape is described as the sum of two Gaussian functions with a common mean, and the background is parameterised as a first-order polynomial. The fit is shown in Fig. 1. The selected Λ_c^+ yield in the full $0.65\,\mathrm{fb}^{-1}$ sample is $N_{\mathrm{norm}} = (818 \pm 7) \times 10^3$, with an invariant mass resolution of around $6\,\mathrm{MeV}/c^2$.

The Ξ_{cc}^+ signal yield is measured from the δm distribution under a series of different mass hypotheses. Although the methods used are designed not to require detailed knowledge of the signal shape, it is necessary to know the resolution with sufficient precision to define

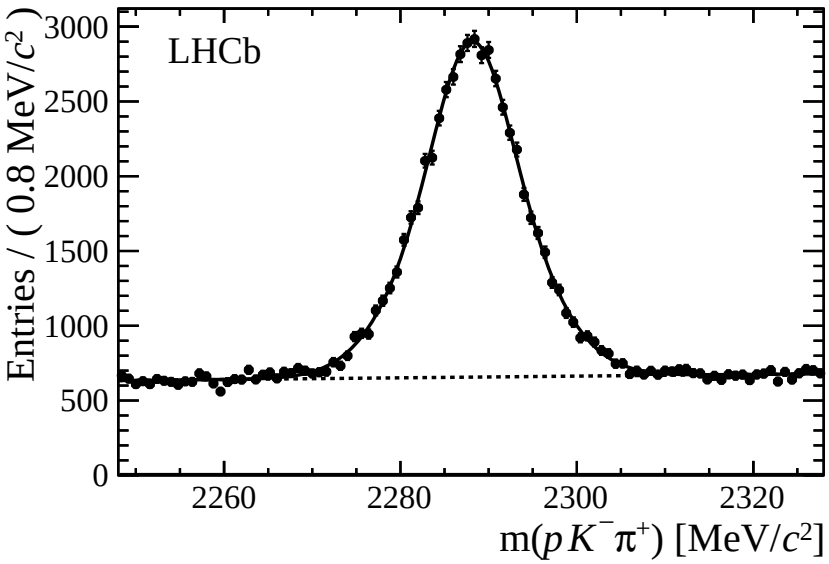

Figure 1: Invariant mass spectrum of $\Lambda_c^+ \to pK^-\pi^+$ candidates for 5% of the data, with events chosen at random during preselection (due to bandwidth limits for the normalisation mode). The dashed line shows the fitted background contribution, and the solid line the sum of Λ_c^+ signal and background.

a signal window. Since the Ξ_{cc}^+ yield may be small, its resolution cannot be measured from data and is instead estimated with a sample of simulated events, shown in Fig. 2. Fitting the candidates with the sum of two Gaussian functions, the resolution is found to be approximately $4.4\,\mathrm{MeV}/c^2$.

Two complementary procedures are used to estimate the signal yield given a mass hypothesis δm_0. Both follow the same general approach, but use different methods to estimate the background. In both cases, a narrow signal window is defined as $2273 < m([pK^-\pi^+]_{\Lambda_c}) < 2303\,\mathrm{MeV}/c^2$ and $|\delta m - \delta m_0| < 10\,\mathrm{MeV}/c^2$, and the number of candidates inside that window is taken as N_{S+B}. Candidates outside the narrow window are used to estimate the expected background N_B inside the window. The signal yield is then $N_S = N_{S+B} - N_B$. This avoids any need to model the signal shape beyond an efficiency correction for the estimated signal fraction lost outside the window of width $20\,\mathrm{MeV}/c^2$.

The first method is an analytic, two-dimensional sideband subtraction in $m([pK^-\pi^+]_{\Lambda_c})$ and δm. A two-dimensional region of width $80\,\mathrm{MeV}/c^2$ in $m([pK^-\pi^+]_{\Lambda_c})$ and width $200\,\mathrm{MeV}/c^2$ in δm is centred around the narrow signal window. A 5×5 array of non-overlapping bins is defined within this region, with the central bin identical to the narrow signal window. It is assumed that the background consists of a combinatorial component, which is described by a two-dimensional quadratic function, and a Λ_c^+ component, which is described by the product of a signal peak in $m([pK^-\pi^+]_{\Lambda_c})$ and a quadratic function in δm. Under this assumption, the background distribution can be fully determined from the

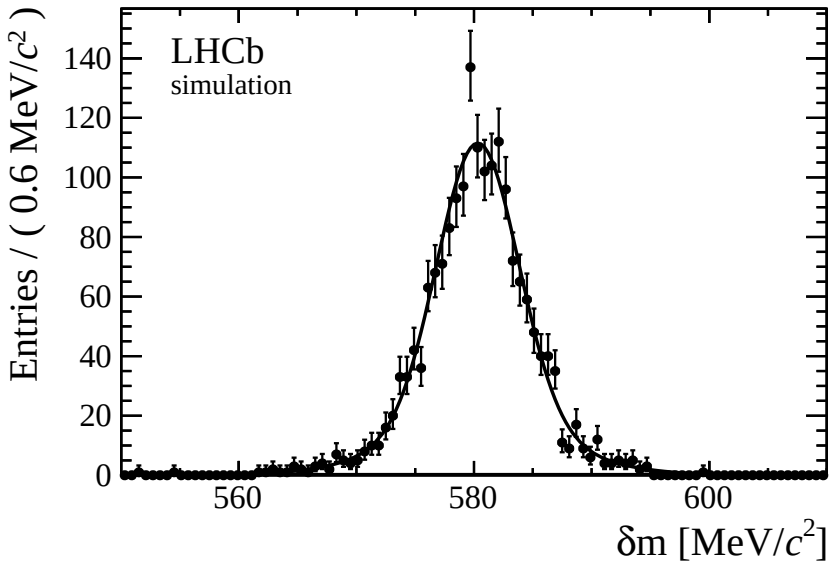

Figure 2: The distribution of the invariant mass difference δm, defined in Eq. 3, for simulated Ξ_{cc}^+ events with a Ξ_{cc}^+ mass of 3500 MeV/c^2. The solid line shows the fitted signal shape. In order to increase the available statistics, the trigger and ANN requirements are not applied in this plot.

24 sideband bins and hence its integral within the signal box calculated. In this way the value of N_B and the associated statistical uncertainty are determined. This method has the advantage that it requires only minor assumptions about the background distribution, given that part of that distribution cannot be studied prior to unblinding. It is adopted as the baseline approach for this reason.

The second method, used as a cross-check, imposes a narrow window on all candidates of $2273 < m([pK^-\pi^+]_{\Lambda_c}) < 2303\,\text{MeV}/c^2$ to reduce the problem to a one-dimensional distribution in δm. Based on studies of the $m([pK^-\pi^+]_{\Lambda_c})$ and δm sidebands, it is found that the background can be described by a function of the form

$$f(\delta m) = \begin{cases} L(\delta m; \mu, \sigma_L) & \delta m \leq \mu \\ aL(\delta m; \mu, \sigma_R) & \delta m \geq \mu \end{cases} \tag{4}$$

where $L(\delta m; \mu, \sigma)$ is a Landau distribution, a is chosen such that $L(\mu; \mu, \sigma_L) = aL(\mu; \mu, \sigma_R)$, and μ, σ_L, and σ_R are free parameters. The data are fitted with this function across the full range, $0 < \delta m < 1500\,\text{MeV}/c^2$, excluding the signal window of width $20\,\text{MeV}/c^2$. The fit function is then integrated across the signal window to give the expected background N_B.

5 Efficiency ratio

To measure R, it is necessary to evaluate the ratio of efficiencies for the normalisation and signal modes, $\varepsilon_{\rm norm}/\varepsilon_{\rm sig}$. The method used to evaluate this ratio is described below. The signal efficiency depends upon the mass and lifetime of the Ξ_{cc}^+, neither of which is known. To handle this, simulated events are generated with $m(\Xi_{cc}^+) = 3500\,\mathrm{MeV}/c^2$ and $\tau_{\Xi_{cc}^+} = 333\,\mathrm{fs}$ and the efficiency ratio is evaluated at this working point. The variation of the efficiency ratio as a function of δm and $\tau_{\Xi_{cc}^+}$ relative to the working point is then determined with a reweighting technique as discussed in Sec. 7. The kinematic distribution of Ξ_{cc}^+ produced at the LHC is also unknown, but unlike the mass and lifetime it cannot be described in a model-independent way with a single additional parameter. Instead, the upper limits are evaluated assuming the distributions produced by the GENXICC model.

The efficiency ratio may be factorised into several components as

$$\frac{\varepsilon_{\rm norm}}{\varepsilon_{\rm sig}} = \frac{\varepsilon_{\rm norm}^{\rm acc}}{\varepsilon_{\rm sig}^{\rm acc}} \frac{\varepsilon_{\rm norm}^{\rm sel|acc}}{\varepsilon_{\rm sig}^{\rm sel|acc}} \frac{\varepsilon_{\rm norm}^{\rm PID|sel}}{\varepsilon_{\rm sig}^{\rm PID|sel}} \frac{1}{\varepsilon_{\rm sig}^{\rm ANN|PID}} \frac{\varepsilon_{\rm norm}^{\rm trig|PID}}{\varepsilon_{\rm sig}^{\rm trig|ANN}}, \tag{5}$$

where efficiencies are evaluated for the acceptance (acc), the reconstruction and selection excluding PID and the ANN (sel), the particle identification cuts (PID), the ANN selector (ANN) for the signal mode only, and the trigger (trig). Each element is the efficiency relative to all previous steps in the order given above.

In most cases the individual ratios are evaluated with simulated Ξ_{cc}^+ and Λ_c^+ decays, taking the fraction of candidates that passed the requirement in question. However, in some cases the efficiencies need to be corrected for known differences between simulation and data. This applies to the efficiencies for tracking, for passing PID requirements, and for passing the calorimeter hardware trigger. Control samples of data are used to determine these corrections as a function of track kinematics and event charged track multiplicity, and the simulated events are weighted accordingly. The data samples used are $J/\psi \to \mu^+\mu^-$ for the tracking efficiency, and $D^{*+} \to D^0(\to K^-\pi^+)\pi^+$ and $\Lambda \to p\pi^-$ for both the PID and calorimeter hardware trigger requirements. The track multiplicity distribution is taken from data for the Λ_c^+ sample, but for Ξ_{cc}^+ events it is not known. It is modelled by taking a sample of events containing a reconstructed B_s^0 decay, on the grounds that B_s^0 production also requires two non-light quark-antiquark pairs.

The efficiency ratio obtained at this working point is $\varepsilon_{\rm norm}/\varepsilon_{\rm sig} = 20.4$. Together with the value for $N_{\rm norm}$ obtained in Sec. 4 and the definition in eq. 2, this implies the single-event sensitivity α is 2.5×10^{-5} at $m(\Xi_{cc}^+) = 3500\,\mathrm{MeV}/c^2$, $\tau_{\Xi_{cc}^+} = 333\,\mathrm{fs}$.

6 Systematic uncertainties

The statistical uncertainty on the measured signal yield is the dominant uncertainty in this analysis, and the systematic uncertainties on α have very limited effect on the expected upper limits. As in the previous section, they will be evaluated at the working point of $m(\Xi_{cc}^+) = 3500\,\mathrm{MeV}/c^2$ and $\tau_{\Xi_{cc}^+} = 333\,\mathrm{fs}$, and their variation with mass and lifetime

Table 1: Systematic uncertainties on the single-event sensitivity α.

Source	Size
Simulated sample size	18.0%
IP resolution	13.3%
PID calibration	11.8%
Tracking efficiency	4.7%
Trigger efficiency	3.3%
Total uncertainty	26.0%

hypothesis considered separately. Of the systematic uncertainties, the largest (18.0%) is due to the limited sample size of simulated events used to calculate the efficiency ratio. Beyond this, there are several instances where the simulation may not describe the signal accurately in data. These are corrected with control samples of data, with systematic uncertainties, outlined below, assigned to reflect uncertainties in these corrections.

The IP resolution of tracks in the VELO is found to be worse in data than in simulated events. To estimate the impact of this effect on the signal efficiency, a test is performed with simulated events in which the VELO resolution is artificially degraded to the same level. This is found to change the efficiency of the reconstruction and non-ANN selection by 6.6%, and that of the ANN by 6.7%. Taking these effects to be fully correlated, a systematic uncertainty of 13.3% is assigned.

A track-by-track correction is applied to the PID efficiency based on control samples of data. There are several systematic uncertainties associated with this correction. The first is due to the limited size of the control samples, notably for high-$p_{\rm T}$ protons from the Λ sample. The second is due to the assumption that the corrections factorise between the tracks, whereas in practice there are kinematic correlations. The third is due to the dependence on the event track multiplicity. The fourth is due to limitations in the method (*e.g.* the finite kinematic binning used) and is assessed by applying it to samples of simulated events. The sum in quadrature of the above gives an uncertainty of 11.8%.

Systematic uncertainties also arise from the tracking efficiency (4.7%) and from the hardware trigger efficiency (3.3%). Additional systematic uncertainties associated with candidate multiplicity, yield measurement, and the decay model of $\Xi_{cc}^{+} \to \Lambda_c^{+} K^{-} \pi^{+}$, which may proceed through intermediate resonances, were considered but found to be negligible in comparison with the total systematic uncertainty. The systematic uncertainties are summarised in Table 1. Taking their sum in quadrature, the total systematic uncertainty is 26%.

Table 2: Single-event sensitivity α for different lifetime hypotheses τ, assuming $m(\Xi_{cc}^+) = 3500\,\mathrm{MeV}/c^2$. The uncertainties quoted include statistical and systematic effects, and are correlated between different lifetime hypotheses.

τ	$\alpha\,(\times 10^{-5})$
100 fs	63 ± 31
150 fs	15 ± 5
250 fs	4.1 ± 1.1
333 fs	2.5 ± 0.6
400 fs	1.9 ± 0.5

7 Variation of efficiency with mass and lifetime

The efficiency to trigger on, reconstruct, and select Ξ_{cc}^+ candidates has a strong dependence upon the Ξ_{cc}^+ lifetime. The efficiency also depends upon the Ξ_{cc}^+ mass, since this affects the opening angles and the p_T of the daughters.

The simulated Ξ_{cc}^+ events are generated with a proper decay time distribution given by an exponential function of average lifetime $\tau_{\Xi_{cc}^+} = 333\,\mathrm{fs}$. To test other lifetime hypotheses, the simulated events are reweighted to follow a different exponential distribution and the efficiency is recomputed. Most systematic uncertainties are unaffected, but those associated with the limited simulated sample size and with the hardware trigger efficiency increase at shorter lifetimes (the latter due to kinematic correlations rather than direct dependence on the decay time distribution). The values and uncertainties of the single-event sensitivity α are given for several lifetime hypotheses in Table 2.

To assess the effect of varying the Ξ_{cc}^+ mass hypothesis, large samples of simulated events are generated for two other mass hypotheses, $m(\Xi_{cc}^+) = 3300\,\mathrm{MeV}/c^2$ and $3700\,\mathrm{MeV}/c^2$, without running the GEANT4 detector simulation. Two tests are carried out with these samples. First, the detector acceptance efficiency is recalculated. Second, the p_T distributions of the three daughters of the Ξ_{cc}^+ in the main $m(\Xi_{cc}^+) = 3500\,\mathrm{MeV}/c^2$ sample are reweighted to match those seen at the other mass hypotheses and the remainder of the efficiency is recalculated. In both cases the systematic uncertainties are also recalculated, though very little change is found. Significant variations in individual components of the efficiency are seen—notably in the acceptance, reconstruction, non-ANN selection, and hardware trigger efficiencies—but when combined cancel almost entirely. This is shown in Table 3, which gives the value of α including the mass-dependent effects discussed above but excluding the correction for the efficiency of the δm signal window described in Sec. 4 (α_u), the correction for the variation in resolution, and the combined value of α. Because the variation of α_u with mass is extremely small, a simple first-order correction is sufficient. A straight line is fitted to the three points in the table and used to interpolate the fractional variation in α_u between the mass hypotheses. The resolution correction is then applied separately. Due to the smallness of the mass-dependence, correlations

Table 3: Variation in single-event sensitivity for different mass hypotheses $m(\Xi_{cc}^+)$, assuming $\tau = 333\,\text{fs}$. The uncertainties quoted include statistical and systematic effects, and are correlated between different mass hypotheses. The variation is shown separately for all effects other than the efficiency of the δm window (α_u), for the correction due to the mass-dependent resolution, and for the combination (α).

$m(\Xi_{cc}^+)$	$\alpha_u\,(\times 10^{-5})$	Resolution correction	$\alpha\,(\times 10^{-5})$
$3300\,\text{MeV}/c^2$	2.29 ± 0.61	0.992	2.30 ± 0.62
$3500\,\text{MeV}/c^2$	2.38 ± 0.62	0.957	2.49 ± 0.65
$3700\,\text{MeV}/c^2$	2.36 ± 0.63	0.903	2.61 ± 0.70

Table 4: Expected value of the signal yield N_{sig} for different values of R and lifetime hypotheses, assuming $m(\Xi_{cc}^+) = 3500\,\text{MeV}/c^2$. The uncertainties quoted are due to the systematic uncertainty on α.

τ	$R = 9\%$	$R = 10^{-4}$	$R = 10^{-5}$
100 fs	140 ± 70	0.2 ± 0.1	0.02 ± 0.01
150 fs	600 ± 200	0.7 ± 0.2	0.07 ± 0.02
250 fs	2200 ± 600	2.4 ± 0.7	0.24 ± 0.07
333 fs	3600 ± 900	4.0 ± 1.0	0.40 ± 0.10
400 fs	4800 ± 1200	5.3 ± 1.4	0.53 ± 0.14

between variation with mass and with lifetime are neglected.

As explained in Sec. 1, the value of R at LHCb is not well known but is expected to be of the order 10^{-5} to 10^{-4}, while the SELEX observation corresponds to $R = 9\%$. Table 4 shows the expected signal yield, calculated according to eq. 1, for various values of R and lifetime hypotheses. From studies of the sidebands in $m([pK^-\pi^+]_{\Lambda_c})$ and δm, the expected background in the narrow signal window is between 10 and 20 events. Thus, no significant signal excess is expected if the value of R at LHCb is in the range suggested by theory. However, if production is greatly enhanced for baryon-baryon collisions at high rapidity, as reported at SELEX, a large signal may be visible. The procedure for determining the significance of a signal, or for establishing limits on R, is discussed in the following section.

8 Tests for statistical significance and upper limit calculation

Since $m(\Xi_{cc}^+)$ is *a priori* unknown, tests for the presence of a signal are carried out at numerous mass hypotheses, between $\delta m = 380\,\text{MeV}/c^2$ and $\delta m = 880\,\text{MeV}/c^2$ inclusive in

$1\,\mathrm{MeV}/c^2$ steps for a total of 501 tests. For a given value of δm, the signal and background yields and their associated statistical uncertainties are estimated as described in Sec. 4. From these the local significance $\mathcal{S}(\delta m)$ is calculated, where $\mathcal{S}(\delta m)$ is defined as

$$\mathcal{S}(\delta m) \equiv \frac{N_{S+B} - N_B}{\sqrt{\sigma_{S+B}^2 + \sigma_B^2}} \tag{6}$$

and σ_{S+B} and σ_B are the estimated statistical uncertainties on the yield in the signal window and on the expected background, respectively. Since multiple points are sampled, the look elsewhere effect (LEE) [39] must be taken into account. The procedure used is to generate a large number of pseudo-experiments containing only background events, with the amount and distribution of background chosen to match the data (as estimated from sidebands). For each pseudo-experiment, the full analysis procedure is applied in the same way as for data, and the local significance is measured at all 501 values of δm. The LEE-corrected p-value for a given $\mathcal{S}$ is then taken to be the fraction of the pseudo-experiments that contain an equal or larger local significance at any point in the δm range.

The procedure established before unblinding is that if no signal with an LEE-corrected significance of at least 3σ is seen, upper limits on R will be quoted. The CL_s method [40,41] is applied to determine upper limits on R for a particular δm and lifetime hypothesis, given the observed yield N_{S+B} and expected background N_B in the signal window obtained as described in Sec. 4. The statistical uncertainty on N_B and systematic uncertainties on α are taken into account. The 95% CL upper limit is then taken as the value of R for which $CL_s = 0.05$. Upper limits are calculated at each of the 501 δm hypotheses, and for five lifetime hypotheses (100, 150, 250, 333, 400 fs).

9 Results

The δm spectrum in data is shown in Fig. 3, and the estimated signal yield in Fig. 4. No clear signal is found with either background subtraction method. In both cases the largest local significance occurs at $\delta m = 513\,\mathrm{MeV}/c^2$, with $\mathcal{S} = 1.5\sigma$ in the baseline method and $\mathcal{S} = 2.2\sigma$ in the cross-check. Applying the LEE correction described in Sec. 8, these correspond to p-values of 99% and 53%, respectively. Thus, with no significant excess found above background, upper limits are set on R at the 95% CL, shown in Fig. 5 for the first method. These limits are tabulated in Table 5 for blocks of δm and the five lifetime hypotheses. The blocks are $50\,\mathrm{MeV}/c^2$ wide, and for each block the largest (worst) upper limit seen for a δm point in that block is given. Similarly, the largest upper limit seen in the entire $500\,\mathrm{MeV}/c^2$ mass range is also given. A strong dependence in sensitivity on the lifetime hypothesis is seen.

The decay $\Xi_{cc}^+ \to \Lambda_c^+ K^- \pi^+$ may proceed through an intermediate Σ_c^{++} resonance. Such decays would be included in the yields and limits already shown. Nonetheless, further checks are made with an explicit requirement that the $\Lambda_c^+ \pi^+$ invariant mass be consistent with that of a Σ_c^{++}, since this substantially reduces the combinatorial background. For

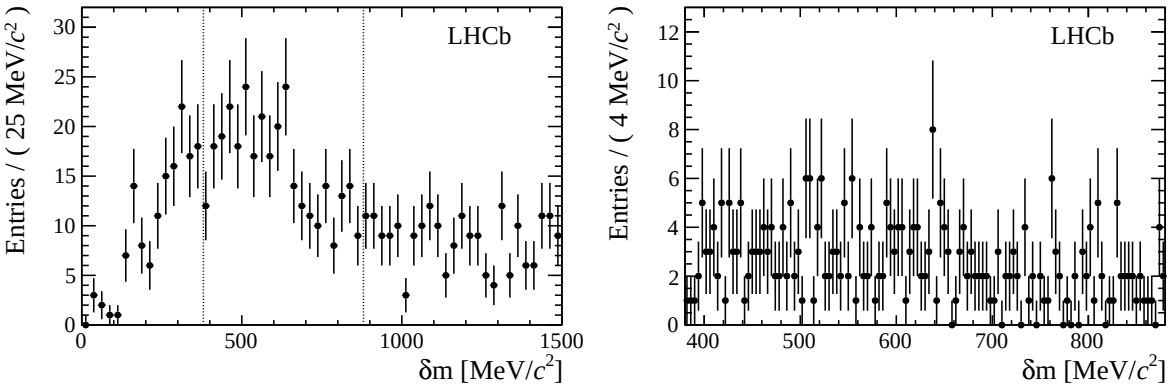

Figure 3: Spectrum of δm requiring $2273 < m([pK^-\pi^+]_{\Lambda_c}) < 2303\,\text{MeV}/c^2$. Both plots show the same data sample, but with different δm ranges and binnings. The wide signal region is shown in the right plot and indicated by the dotted vertical lines in the left plot.

Table 5: Largest values of the upper limits (UL) on R at the 95% CL in blocks of δm for a range of lifetime hypotheses, given in units of 10^{-3}. The largest values across the entire $500\,\text{MeV}/c^2$ range are also shown.

	R, largest 95% CL UL in range $\times 10^3$				
δm (MeV/c^2)	100 fs	150 fs	250 fs	333 fs	400 fs
380–429	12.6	2.7	0.73	0.43	0.33
430–479	11.2	2.4	0.65	0.39	0.29
480–529	14.8	3.2	0.85	0.51	0.39
530–579	10.7	2.3	0.63	0.38	0.29
580–629	10.9	2.3	0.63	0.38	0.29
630–679	14.2	3.0	0.81	0.49	0.37
680–729	9.5	2.0	0.56	0.33	0.25
730–779	10.8	2.3	0.63	0.37	0.28
780–829	12.8	2.8	0.74	0.45	0.34
830–880	12.2	2.6	0.70	0.42	0.32
380–880	14.8	3.2	0.85	0.51	0.39

$\Sigma_c(2455)^{++}$ and $\Sigma_c(2520)^{++}$, the mass offsets $[m([pK^-\pi^+]_{\Lambda_c}\pi^+) - m([pK^-\pi^+]_{\Lambda_c})]$ are required to be within $4\,\text{MeV}/c^2$ and $15\,\text{MeV}/c^2$ of the world-average value, respectively. The resulting δm spectra are shown in Fig. 6. No statistically significant excess is present.

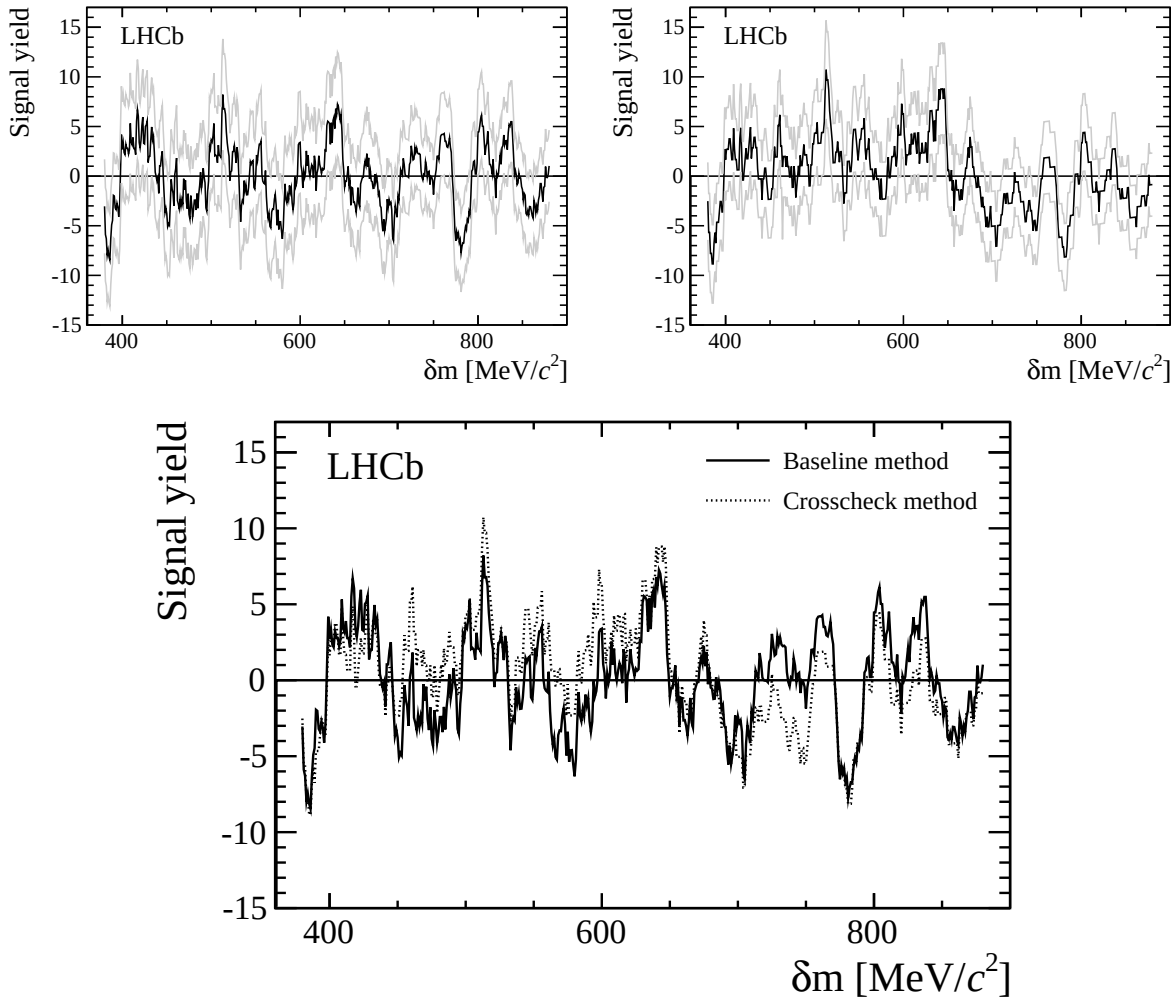

Figure 4: Measured signal yields as a function of δm. The upper two plots show the estimated signal yield as a dark line and the $\pm 1\sigma$ statistical error bands as light grey lines for (upper left) the baseline method and (upper right) the cross-check method. The central values of the two methods are compared in the lower plot and found to agree well.

10 Conclusions

A search for the decay $\Xi_{cc}^+ \to \Lambda_c^+ K^- \pi^+$ is performed at LHCb with a data sample of pp collisions, corresponding to an integrated luminosity of $0.65\,\text{fb}^{-1}$, recorded at a centre-of-mass energy of 7 TeV. No significant signal is found. Upper limits on the Ξ_{cc}^+ cross-section times branching fraction relative to the Λ_c^+ cross-section are obtained for a range of mass and lifetime hypotheses, assuming that the kinematic distributions of the Ξ_{cc}^+ follow those of the GENXICC model. The upper limit depends strongly on the lifetime, varying from 1.5×10^{-2} for 100 fs to 3.9×10^{-4} for 400 fs. These limits are significantly below the value

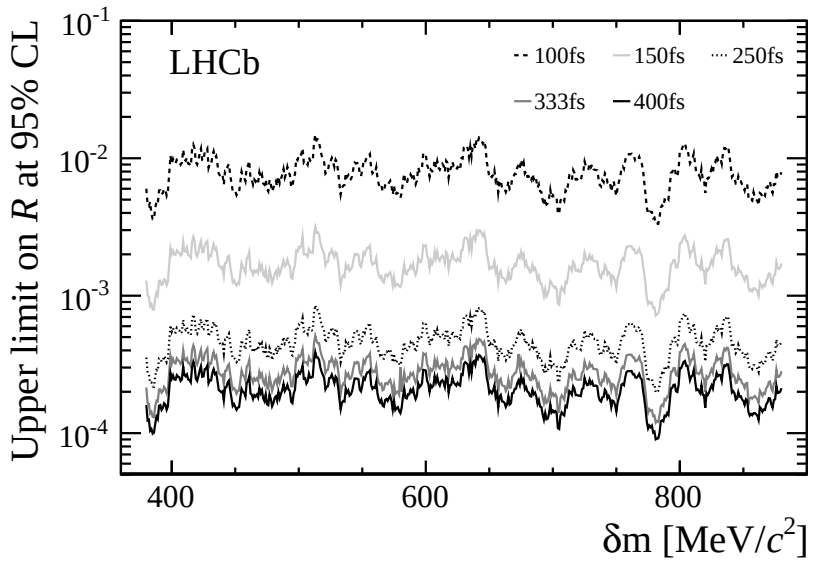

Figure 5: Upper limits on R at the 95% CL as a function of δm, for five Ξ_{cc}^{+} lifetime hypotheses.

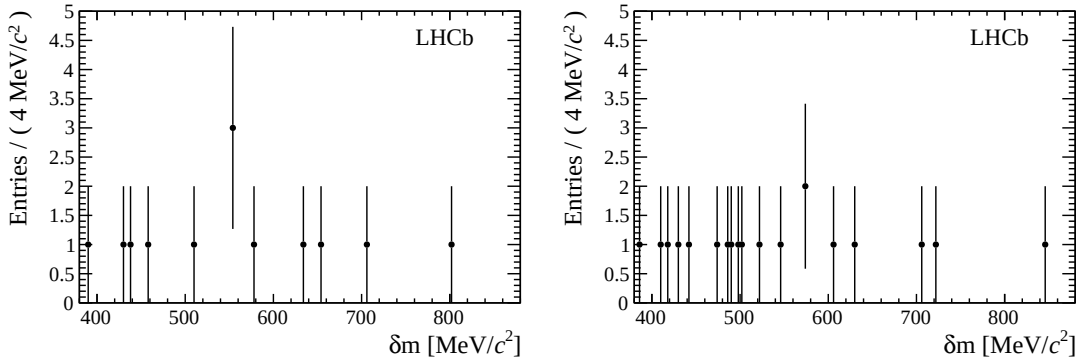

Figure 6: Mass difference spectrum requiring $2273 < m([pK^-\pi^+]_{\Lambda_c}) < 2303\,\mathrm{MeV}/c^2$. Candidates are also required to be consistent with (left) an intermediate $\Sigma_c(2455)^{++}$, (right) an intermediate $\Sigma_c(2520)^{++}$.

of R found at SELEX. This may be explained by the different production environment, or if the Ξ_{cc}^{+} lifetime is indeed very short ($\ll 100\,\mathrm{fs}$). Future searches at LHCb with improved trigger conditions, additional Ξ_{cc} decay modes, and larger data samples should improve the sensitivity significantly, especially at short lifetimes.

Acknowledgements

We express our gratitude to our colleagues in the CERN accelerator departments for the excellent performance of the LHC. We thank the technical and administrative staff at the LHCb institutes. We acknowledge support from CERN and from the national agencies: CAPES, CNPq, FAPERJ and FINEP (Brazil); NSFC (China); CNRS/IN2P3 and Region Auvergne (France); BMBF, DFG, HGF and MPG (Germany); SFI (Ireland); INFN (Italy); FOM and NWO (The Netherlands); SCSR (Poland); MEN/IFA (Romania); MinES, Rosatom, RFBR and NRC "Kurchatov Institute" (Russia); MinECo, XuntaGal and GENCAT (Spain); SNSF and SER (Switzerland); NAS Ukraine (Ukraine); STFC (United Kingdom); NSF (USA). We also acknowledge the support received from the ERC under FP7. The Tier1 computing centres are supported by IN2P3 (France), KIT and BMBF (Germany), INFN (Italy), NWO and SURF (The Netherlands), PIC (Spain), GridPP (United Kingdom). We are thankful for the computing resources put at our disposal by Yandex LLC (Russia), as well as to the communities behind the multiple open source software packages that we depend on.

References

[1] M. Gell-Mann, *A schematic model of baryons and mesons*, Phys. Lett. **8** (1964) 214.

[2] G. Zweig, *An SU(3) model for strong interaction symmetry and its breaking, Part 1*, 1964. CERN-TH-401.

[3] G. Zweig, *An SU(3) model for strong interaction symmetry and its breaking, Part 2*, 1964. CERN-TH-412, Published in 'Developments in the Quark Theory of Hadrons'. Volume 1. Edited by D. Lichtenberg and S. Rosen. Nonantum, Mass., Hadronic Press, 1980. pp. 22-101.

[4] A. De Rujula, H. Georgi, and S. Glashow, *Hadron masses in a gauge theory*, Phys. Rev. **D12** (1975) 147.

[5] Particle Data Group, J. Beringer *et al.*, *Review of particle physics*, Phys. Rev. **D86** (2012) 010001, and 2013 partial update for the 2014 edition.

[6] W. Roberts and M. Pervin, *Heavy baryons in a quark model*, Int. J. Mod. Phys. **A23** (2008) 2817, `arXiv:0711.2492`.

[7] D.-H. He *et al.*, *Evaluation of spectra of baryons containing two heavy quarks in bag model*, Phys. Rev. **D70** (2004) 094004, `arXiv:hep-ph/0403301`.

[8] Z.-G. Wang, *Analysis of the $\frac{1}{2}^+$ doubly heavy baryon states with QCD sum rules*, Eur. Phys. J. **A45** (2010) 267, `arXiv:1001.4693`.

[9] C.-H. Chang, C.-F. Qiao, J.-X. Wang, and X.-G. Wu, *Estimate of the hadronic production of the doubly charmed baryon Ξ_{cc} under GM-VFN scheme*, Phys. Rev. **D73** (2006) 094022, arXiv:hep-ph/0601032.

[10] A. Valcarce, H. Garcilazo, and J. Vijande, *Towards an understanding of heavy baryon spectroscopy*, Eur. Phys. J. **A37** (2008) 217, arXiv:0807.2973.

[11] J.-R. Zhang and M.-Q. Huang, *Doubly heavy baryons in QCD sum rules*, Phys. Rev. **D78** (2008) 094007, arXiv:0810.5396.

[12] C.-H. Chang, T. Li, X.-Q. Li, and Y.-M. Wang, *Lifetime of doubly charmed baryons*, Commun. Theor. Phys. **49** (2008) 993, arXiv:0704.0016.

[13] D. Ebert, R. Faustov, V. Galkin, and A. Martynenko, *Mass spectra of doubly heavy baryons in the relativistic quark model*, Phys. Rev. **D66** (2002) 014008, arXiv:hep-ph/0201217.

[14] B. Guberina, B. Melic, and H. Stefancic, *Inclusive decays and lifetimes of doubly charmed baryons*, Eur. Phys. J. **C9** (1999) 213, arXiv:hep-ph/9901323.

[15] SELEX collaboration, M. Mattson *et al.*, *First observation of the doubly charmed baryon Ξ_{cc}^+*, Phys. Rev. Lett. **89** (2002) 112001, arXiv:hep-ex/0208014.

[16] SELEX collaboration, A. Ocherashvili *et al.*, *Confirmation of the double charm baryon $\Xi_{cc}^+(3520)$ via its decay to pD^+K^-*, Phys. Lett. **B628** (2005) 18, arXiv:hep-ex/0406033.

[17] V. Kiselev and A. Likhoded, *Baryons with two heavy quarks*, Phys. Usp. **45** (2002) 455, arXiv:hep-ph/0103169.

[18] S. Ratti, *New results on c-baryons and a search for cc-baryons in FOCUS*, Nucl. Phys. Proc. Suppl. **115** (2003) 33.

[19] BaBar collaboration, B. Aubert *et al.*, *Search for doubly charmed baryons Ξ_{cc}^+ and Ξ_{cc}^{++} in BaBar*, Phys. Rev. **D74** (2006) 011103, arXiv:hep-ex/0605075.

[20] Belle collaboration, R. Chistov *et al.*, *Observation of new states decaying into $\Lambda_c^+ K^- \pi^+$ and $\Lambda_c^+ K_S^0 \pi^-$*, Phys. Rev. Lett. **97** (2006) 162001, arXiv:hep-ex/0606051.

[21] LHCb collaboration, R. Aaij *et al.*, *Observation of J/ψ-pair production in pp collisions at $\sqrt{s} = 7\ TeV$*, Phys. Lett. **B707** (2012) 52, arXiv:1109.0963.

[22] LHCb collaboration, R. Aaij *et al.*, *Observation of double charm production involving open charm in pp collisions at $\sqrt{s} = 7\ TeV$*, JHEP **06** (2012) 141, arXiv:1205.0975.

[23] J. Ma and Z. Si, *Factorization approach for inclusive production of doubly heavy baryon*, Phys. Lett. **B568** (2003) 135, arXiv:hep-ph/0305079.

[24] C.-H. Chang, J.-P. Ma, C.-F. Qiao, and X.-G. Wu, *Hadronic production of the doubly charmed baryon Ξ_{cc} with intrinsic charm*, J. Phys. **G34** (2007) 845, arXiv:hep-ph/0610205.

[25] LHCb collaboration, R. Aaij *et al.*, *Prompt charm production in pp collisions at $\sqrt{s} = 7$ TeV*, Nucl. Phys. **B871** (2013) 1, arXiv:1302.2864.

[26] LHCb collaboration, A. A. Alves Jr. *et al.*, *The LHCb detector at the LHC*, JINST **3** (2008) S08005.

[27] M. Adinolfi *et al.*, *Performance of the LHCb RICH detector at the LHC*, Eur. Phys. J. **C73** (2013) 2431, arXiv:1211.6759.

[28] A. A. Alves Jr *et al.*, *Performance of the LHCb muon system*, JINST **8** (2013) P02022, arXiv:1211.1346.

[29] R. Aaij *et al.*, *The LHCb trigger and its performance in 2011*, JINST **8** (2013) P04022, arXiv:1211.3055.

[30] T. Sjöstrand, S. Mrenna, and P. Skands, *PYTHIA 6.4 physics and manual*, JHEP **05** (2006) 026, arXiv:hep-ph/0603175.

[31] I. Belyaev *et al.*, *Handling of the generation of primary events in* Gauss*, the LHCb simulation framework*, Nuclear Science Symposium Conference Record (NSS/MIC) **IEEE** (2010) 1155.

[32] C.-H. Chang, J.-X. Wang, and X.-G. Wu, *GENXICC2.0: An upgraded version of the generator for hadronic production of double heavy baryons Ξ_{cc}, Ξ_{bc} and Ξ_{bb}*, Comput. Phys. Commun. **181** (2010) 1144, arXiv:0910.4462.

[33] D. J. Lange, *The EvtGen particle decay simulation package*, Nucl. Instrum. Meth. **A462** (2001) 152.

[34] P. Golonka and Z. Was, *PHOTOS Monte Carlo: a precision tool for QED corrections in Z and W decays*, Eur. Phys. J. **C45** (2006) 97, arXiv:hep-ph/0506026.

[35] Geant4 collaboration, J. Allison *et al.*, *Geant4 developments and applications*, IEEE Trans. Nucl. Sci. **53** (2006) 270; Geant4 collaboration, S. Agostinelli *et al.*, *Geant4: a simulation toolkit*, Nucl. Instrum. Meth. **A506** (2003) 250.

[36] M. Clemencic *et al.*, *The LHCb simulation application,* Gauss*: design, evolution and experience*, J. Phys. Conf. Ser. **331** (2011) 032023.

[37] A. Hoecker *et al.*, *TMVA: the Toolkit for Multivariate Data Analysis with ROOT*, PoS **ACAT** (2007) 040, arXiv:physics/0703039.

[38] BaBar collaboration, B. Aubert *et al.*, *Study of excited charm-strange baryons with evidence for new baryons* $\Xi_c(3055)^+$ *and* $\Xi_c(3123)^+$, Phys. Rev. **D77** (2008) 012002, arXiv:0710.5763.

[39] L. Lyons, *Open statistical issues in Particle Physics*, Ann. Appl. Stat. **2** (2008) 887.

[40] A. L. Read, *Presentation of search results: The CL(s) technique*, J. Phys. **G28** (2002) 2693.

[41] G. Cowan, K. Cranmer, E. Gross, and O. Vitells, *Asymptotic formulae for likelihood-based tests of new physics*, Eur. Phys. J. **C71** (2011) 1554, arXiv:1007.1727.